Indian Journal of Pure & Applied Physics
Vol. 61, March 2023, pp. 190-197
DOI: 10.56042/ijpap.v61i3.71091

The Effect of Different Molar Ratios of CeO_2 on Photoluminescence Properties of CeO_2/TiO_2 Nanoparticles

Fatma Kiliç Dokan[a]*, Mehmet Kuru[b], Handan Özlü Torun[c] & Esra Öztürk[d]

[a]Mustafa Çıkrıkcıoğlu Vocational School, Department of Chemistry and Chemical Processing Technologies, Kayseri University, Kayseri, Turkey

[b]Faculty of Engineering, Metallurgy and Materials Engineering Department, Ondokuz Mayıs University, Samsun, Turkey

[c]Department of Energy System Engineering, Kahramanmaraş İstiklal University, 46000, Kahramanmaraş, Turkey

[d]Department of Metallurgical and Materials Engineering, Karamanoglu Mehmetbey University, 70100, Karaman, Turkey

Received 3 February 2023; accepted 27 February 2023

The CeO_2-TiO_2 nanoparticles were prepared by a combination of hydrothermal and sol-gel preparation methods. The bond structures and crystal properties of the obtained materials were featured with X-ray diffraction, FTIR, Raman, and Bet analysis; surface morphologies were examined with the help of FESEM and STEM. And finally, the PL properties of the synthesized samples were also examined in this study. The excitation and emission spectra of 0.1 mol% and 0.25 mol% CeO_2 doped TiO_2 phosphors consist of broad bands in the UV (200–300 nm) region with maxima at 254 nm. The excitation band at 254 nm is defined as the charge transfer band (CTB). In the emission spectra, a broadband located from 400 to 700 nm is related to the 5d-4f (5d1→4f1) transition of Ce^{3+} in TiO_2. According to the PL result, the 5d–4f transition of Ce^{3+} is heavily dependent on the concentration of Ce^{3+} in the host crystal TiO_2.

Keywords: Photoluminescence properties; CeO_2/TiO_2; Nanoparticle

1 Introduction

Combining suitable composites and metal ions to produce new luminescence is an issue that attracts attention today. This interest is due to their interior architectural beauty or aesthetic structure and potential applications in the field of organic light-emitting diodes (OLEDs), lasers, transistors, and fluorescent sensors. It is also crucial for use in highly specific probes[1-5]. TiO_2 has recently become a promising material in various applications such as photocatalysis and photovoltaic. It has a great range of research areas in applications such as photosensors, moisture sensors, and solar cells[6-9]. However, the photocatalytic properties of TiO_2 are limited by the structure and band gap[10]. All studies have shown that TiO_2 is only active under UV light[11].

With all these properties, TiO_2, a semiconductor metal oxide, can be used as an oxygen gas sensor to control the air/fuel mixture in car engines[12-13], and its high dielectric constant greatly expands TiO_2 applications in electronic devices such as capacitors and memory devices. Titanium dioxide pigment is commonly used in almost all paints due to its high refractive index. Interestingly, pure TiO_2 is non-toxic and readily dispersible and can be used in food additives[14], cosmetics, and pharmaceutical agents[15].

The most important development for TiO_2 is that defects in TiO_2 nanostructures attract attention because internal and external defects play a vital and fundamental role in improving material performance. Understanding the origin of the visible light photoactivity of the undoped and doped TiO_2 motivated various studies[16-19]. The photoluminescence properties of TiO_2, as with many materials (PL), are highly dependent on sample synthesis, the presence of additives and defects, and the condition of its surface[20-25].

Crystal structures and improvement of surface properties of TiO_2 also have basic compatibility with its luminescent properties. Therefore, the investigation of TiO_2 by photoluminescence spectroscopy can provide information about surface regions[25-30]. The width and relative intensity of the gloss emission bands are often affected by the nature of the cage. The feature of emission bands depends mainly on the crystal structure. This important parameter can be used to adjust the emission of materials depending on the applications.

*Corresponding authors: (E-mail: fatmakilic@kayseri.edu.tr)

The luminescent properties of rare earths in different compositions are essential[31-32]. How can light be developed effectively due to the multiple light scattering and reflecting effects in the inner space, which is beneficial for luminescence efficiency? Although there are studies on this in the literature, the improvement of photoluminescence properties of TiO_2 by a composite with oxides of rare earth elements has not been investigated[33-36].

Recently rare earths and TiO_2 composites in terms of luminescence properties have gained importance. Several studies reported that rare earth elements in TiO_2 achieved effective results for environmental (water and air) distillation by changing the surface adsorption properties, band gap energy, and the complexity of organic pollutants relative to f-levels[37]. Some researchers reported that the TiO_2 matrix doped with rare-earth ions prevented the e−/h + pair recombination due to the formation of defects. Although there are some reports on this issue, little optimization work has been done[38].

We reported on the synthesis, characterization, and PL performance of CeO_2-TiO_2 nanocomposite.

2 Materials and Methods

TiO_2 microspheres were synthesized adopting the method reported in our previous work[39]. In the synthesis of pure CeO_2/TiO_2 composites, all chemicals used are of analytical grade. The sol-gel method was used for the synthesis of nano-sized CeO_2/TiO_2 composites. The mixing process was done with an ultrasonic mixer and stirring was continued until the alcohol in the solution evaporated, and the solution turned into a gel. The gel mixture was then calcined for six hours at 450 °C, and finally, CeO_2/TiO_2 nanocomposites were synthesized. Field emission scanning electron microscopy and elemental analysis were investigated by EDX (energy dispersive) (FE-SEM, Zeiss); X-ray diffraction (XRD) analysis was performed to determine the crystallinity and phase purity of the samples using XRD (Pananalytic Imperial) with Cu-Kα radiation (l= 1.5406 Å) in the 2Θ range from 20 to 90 with a 0.02 step angle. Fourier transform infrared spectroscopy (FT-IR, Perkin–Elmer-spotlight 400) techniques characterize the prepared CeO_2/TiO_2 nanocomposite. The surface area of the samples was determined by nitrogen adsorption-desorption analysis at (micromeritic-Gemini IV). The photoluminescence spectra were measured by Fluorescence spectrophotometer (HITACHI F-7100). All PL measurements were performed in an open atmosphere and at room temperature.

3 Results

3.1 XRD Analysis

The powder X-ray diffraction (XRD) analysis was performed to determine the crystallinity and phase purity of the samples using Pan analytic Imperial powder diffractometer with Cu Kα radiation. The XRD powder pattern was indexed using Diffrac Plus, Win-Metric programs, and unit cell parameters were calculated. The XRD patterns of TiO_2-CeO_2 nanocomposites are given in Fig. 1. 0.02 step angle in the range of 2 θ = 10–90, at 40 kV and 40 mA. The sharp diffraction peaks at 2θ values indexed the anatase phase of TiO_2 (01-071-1167). When the XRD patterns are examined in detail, as the amount of CeO_2 increases, CeO_2 peaks are observed in the pattern.

The crystallite size measurements were also carried out using the Scherrer equation[40], which is given as Eq. 1, where λ is the wavelength of the x-ray, θ is the X-ray diffraction angle, and β is the highest full width.

$$D = k\lambda / \beta\cos\theta \quad \ldots 1$$

As seen in Table 1, the crystallite size (D_{SCH}) increases with CeO_2 contribution. This increase in crystallite size can be explained because the full peak width at the half maximum (FWHM) values decreases while the CeO_2 addition increases. Mario J. Muñoz-Batista obtained similar results in the CeO_2/TiO_2 nanocomposites produced by different methods[41].

The Scherrer formula only considers the impact of crystallite size on the XRD peak broadening. However, it does not describe the details of the intrinsic strain that occurs in nanocomposites. The Williamsons-Hall (W-H) method is used to calculate

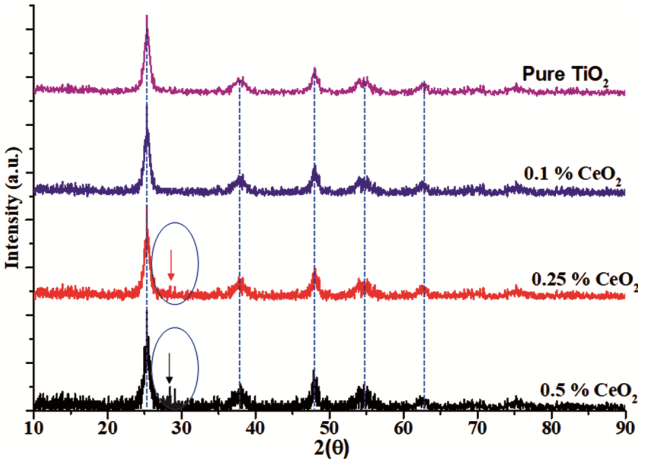

Fig.1 — X-ray diffraction (XRD) patterns of the samples with a different molar ratio.

Table 1 — Crystallite size (from Scherer's equation (D_{SCH}) and Williamson-Hall Plot (D_{W-H}), BET surface area and strain (ε) of TiO_2 and CeO_2-TiO_2 nanocomposites.

Sample	TiO_2	CeO_2-TiO_2 (0.1 %)	CeO_2-TiO_2 (0.25 %)	CeO_2-TiO_2 (0.5%)
D_{SCH} (nm)	8.67	14.18	14.20	14.23
D_{W-H} (nm)	8.99	13.87	13.92	13.87
Surface Area(m^2/g)	36.35	45.75	48.64	62.45
Strain (ε)	0.00181	0.00318	0.00306	0.00305

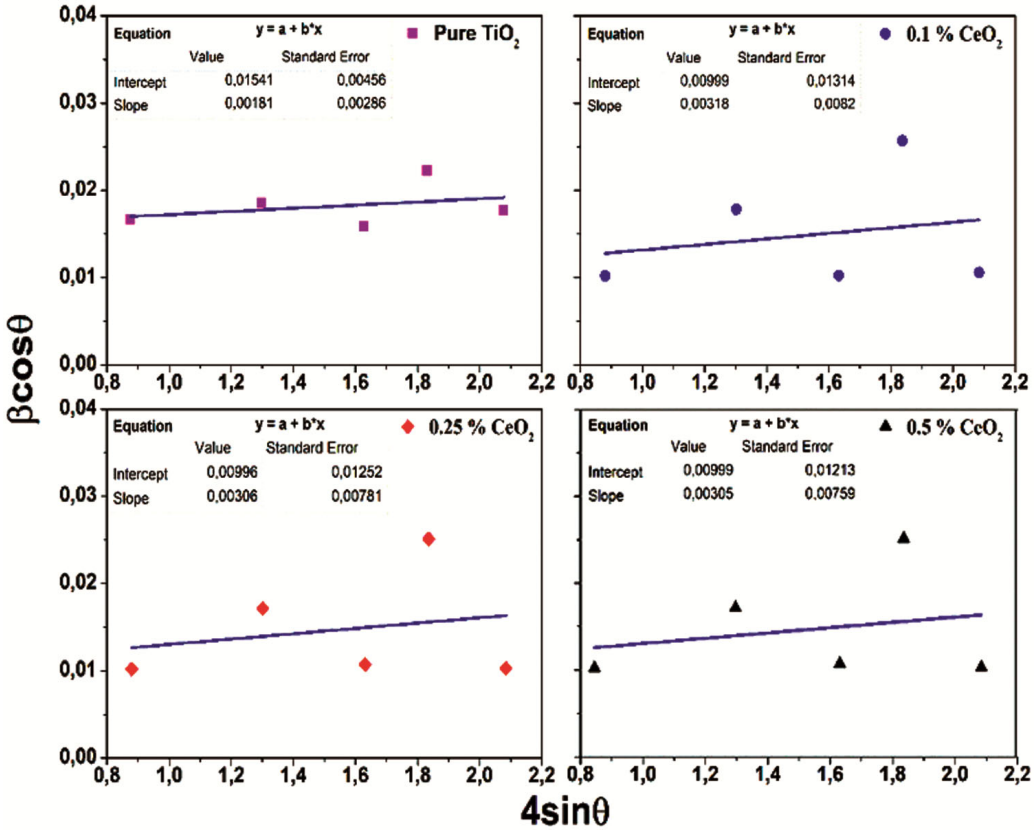

Fig. 2 — Williamson-Hall plots for pure TiO_2 and CeO_2-TiO_2 nanocomposites.

crystal size, intrinsic strain, and consider the effect of XRD peak expansion and strain. The Williamson-Hall plots using the peaks (101), (103), (200), (105), (213), and applied linear fitting are shown in Fig. 2. We calculated the crystallite size (D_{W-H}) and strain (ε) values by plotting $\beta cos\theta$ along the y-axis as a function of $4sin\theta$ on the x-axis corresponding to given diffraction peaks. The slope of this fitting line gives the strain, and the intercept gives the crystal size.

By using the W-H relationship (Eq. 2), the Williamsons-Hall crystallite size (D_{W-H}) and strain were determined[42]. Where k is constant, and ε is the strain-induced inside the nanocomposites.

The crystal sizes obtained from the slope of the W-H plot showed a similar behavior as the results obtained from the Scherer equation, as given in Table 1. When CeO_2 was added to TiO_2, the induced strain increased, but no significant change was observed in the strain value as the CeO_2 contribution increased. This increase in strain may occur due to the difference in the Ce^{4+} (0.92 Å) and Ti^{4+} (0.64 Å) ion radii.

3.2 FTIR and Raman Analysis

FT-IR spectra are shown in Fig. 3(a) in order to examine the bond structures of TiO_2-CeO_2 nanoparticles in the 400–4000 cm^{-1} range. When the spectra are examined,the spectrum exhibits broad absorption peaks between 1600-3400 cm^{-1}, corresponding to the stretching mode of the O-H group of hydroxyl group adsorbed on the surface of nanoparticles. Absorption peaks around 794 are related to Ti-O bonds. The anatase O–Ti–O structure formation was observed as

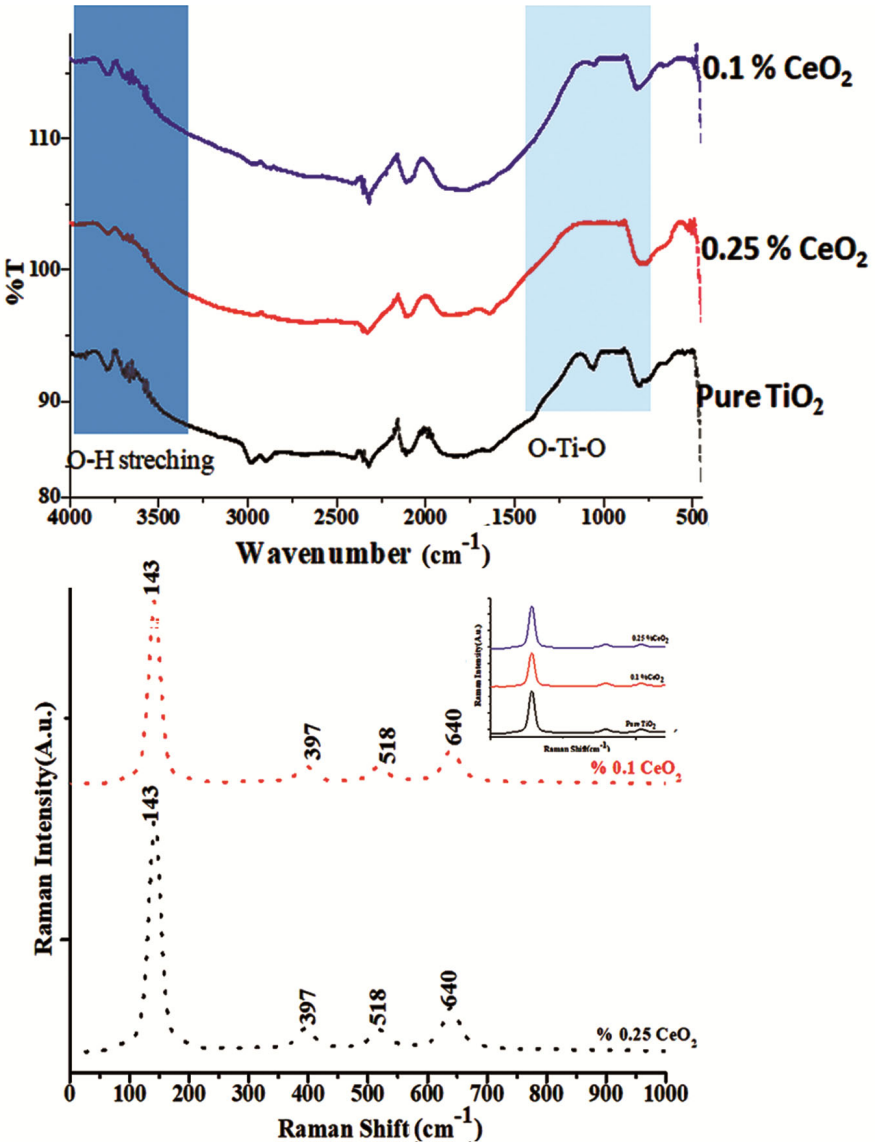

Fig. 3 — (a) Effects of CeO_2 content in CeO_2/TiO_2 nanocomposites on FTIR and b) Raman signals.

a characteristic band with strong and broad absorption in the low energy zone (600–800 cm^{-1})[43,44].

The Raman signals of theTiO_2-CeO_2 nanoparticles are shown in Fig. 3(b). It can be clearly seen that tetragonal TiO_2(A1g + 2B1g + 3Eg) has six active Raman modes 143 cm-1 (Eg), 197 cm-1 (Eg), 397 cm-1 (B1g), 518 cm-1[45] (Alg), 519 cm-1 (B1g), and 640 cm-1 (Eg).The intensities of Raman vibration modes depend on the crystallinity of the oxide, which can vary depending on applied temperature parameters such as pressure and temperature of the furnace during the composite phase-formation process[46]. As seen in the spectra, the change in the amount of CeO_2 was observed with only small shifts in Raman spectra since the amount added was quite low. It was not preferred because the crystal structure changed at higher rates; the anatase structure we showed in our literature research was the most effective structure for PL studies[47-51]. Additionally, high CeO_2 levels were not observed much in Raman and FTIR spectra. Still, only low mole ratios were studied, considering that there may be a missing rutile phase from the XRD spectra.

When the experimental data obtained were evaluated, it was determined that 0.1% and 0.25% doping rates were the optimum values for PL studies.

3.3 FESEM/EDX and S-TEM Analysis

The morphology and structural changes of the CeO_2/TiO_2 nanocomposites are observed by using FE-SEM images, as shown in Fig. 4(a-b). According

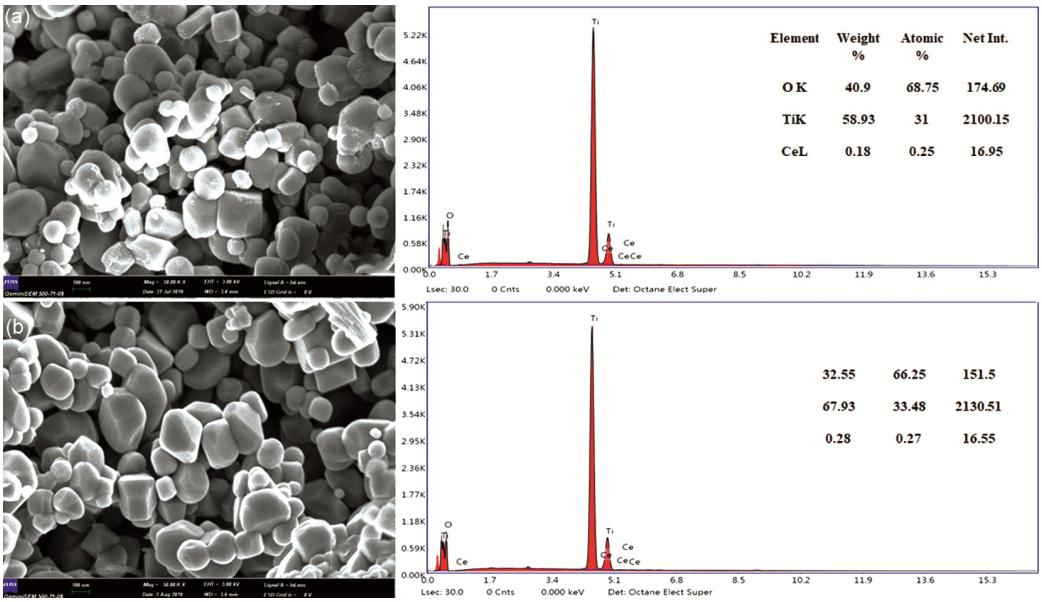

Fig. 4 — (a) 0.1% and b) 0.25 %, CeO_2-TiO_2 nanocomposite FESEM images and EDX analysis.

to FESEM analysis, the surface was rough, and the particles were regular in shape. In Table 2, EDX studies are details of all the elements present in the given nanocomposites. Fig. 3 shows the EDX pattern of different molar CeO_2 content in CeO_2/TiO_2nanocomposites. EDX results confirm the presence of Ce, Ti, and O elements and the absence of impurity elements.

In addition to FESEM images, the crystal structure of nanocomposites was thoroughly investigated using scanning transmission electron microscopy. S-TEM images appeared as cubic CeO_2 nanoparticles were designed on the large spherical surface of TiO_2 nanoparticles. The white sphere or spherical-like structure is due to the presence of TiO_2 nanoparticles, and the white nature nanoparticles are spread/coated over a wide range. Blackhead or circle or cubic / isometric structure is due to CeO_2 particles[52].

Scanning Transmission Electron Microscopy (STEM) micrographs of nanocomposites are shown in Fig. 5(a-b). As shown in the STEM micrographs, nanocomposites, the particles of nanocomposites, have a regular distribution.

3.4 Adsorption-Desorption Measurements

It is known that photoluminescence efficiency is mainly dependent on properties and some parameters such as crystal phase ratio, surface area, phase purity[53]. Therefore, the surface areas of the synthesized nanocomposites were examined by N_2 adsorption/desorption measurements. For this purpose, N_2 gas was passed through the sample for 24

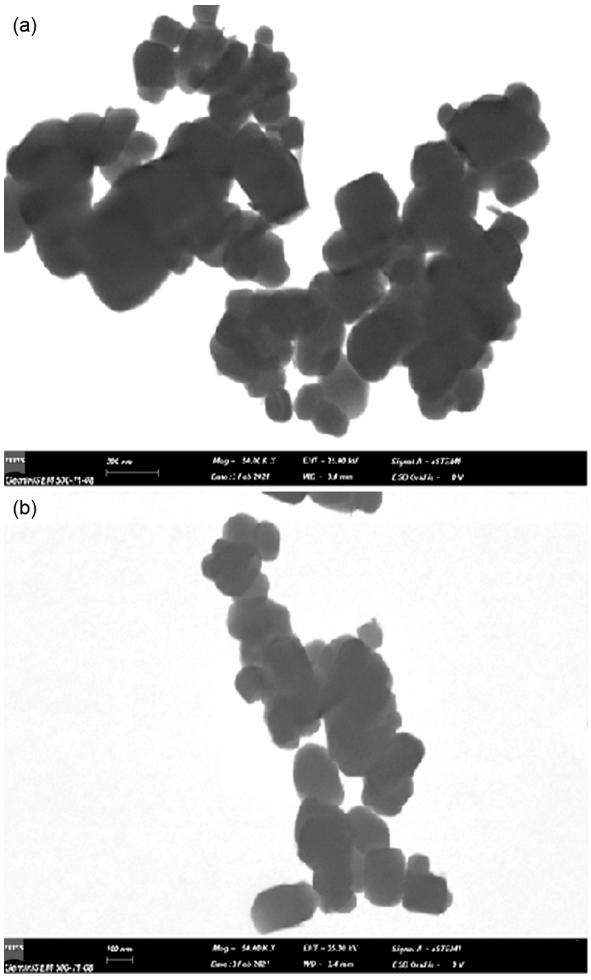

Fig. 5 — (a) 0.1% and b) 0.25 %, CeO_2-TiO_2 nanocomposite S-TEM images.

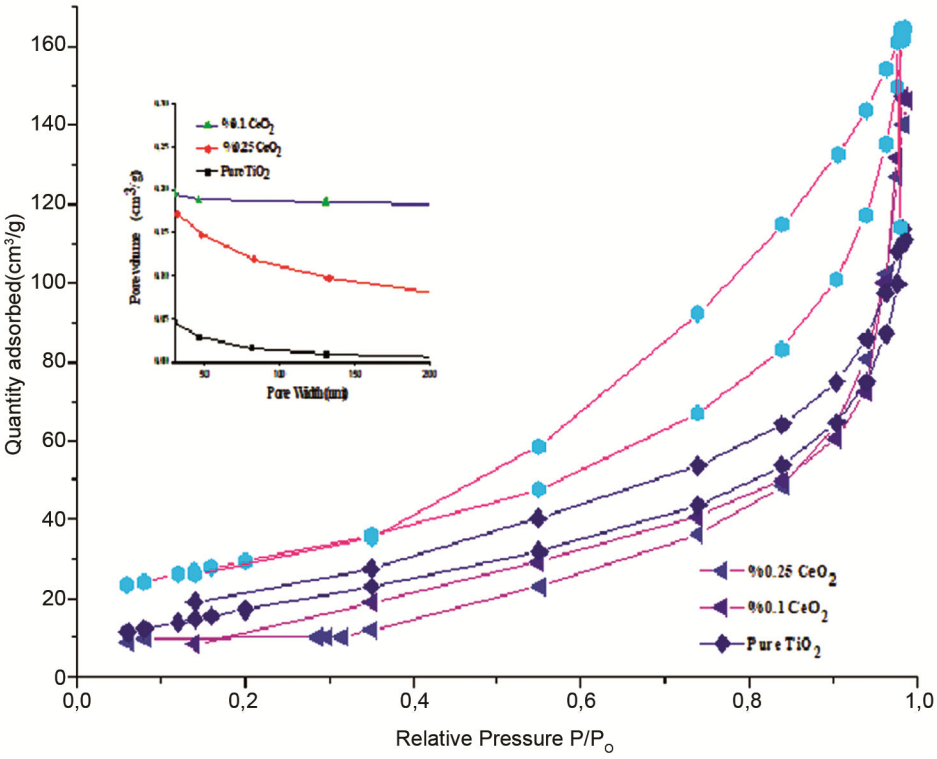

Fig. 6 — Surface area measurements and pore size changes of crystals.

hours to remove the impurities and water vapor in the samples, while the sample cell temperature was at 200 °C. The BET-specific surface areas of the CeO_2 doped samples were observed in the range 36-48m^2g^{-1} (See Table 1). (Fig. 6). The addition of a small amount of CeO_2 caused the doped composite to show a smaller particle size and higher surface area than pure TiO_2, and the reduction in grain size was gradual with the CeO_2 content. This increase may be due to CeO_2-TiO_2 nanocomposite formation, which effectively inhibits boundary mobility and thus grain growth.

3.5 Photoluminescence Properties

The excitation and emission spectra of 0.1 mol% and 0.25 mol% CeO_2 doped TiO_2 phosphors are shown in Fig. 7. The excitation spectra of both phosphors consist of broad bands in the UV (200–300 nm) region with maxima at 254 nm. The excitation band at 254 nm is defined as the charge transfer band (CTB)[54-57]. In the emission spectra, a broad band located from 400 to 700 nm is related to the 5d-4f ($5d^1 \rightarrow 4f^1$) transition of Ce^{3+} in TiO_2. It is known that the emission of Ce^{3+} is heavily affected by the crystal environment. Also, the emission wavelength of Ce^{3+} is very sensitive[58]. The red or blue shift of Ce^{3+} emission is discussed within this framework. In Fig. 7, the maxima of Ce^{3+} emission shifted from

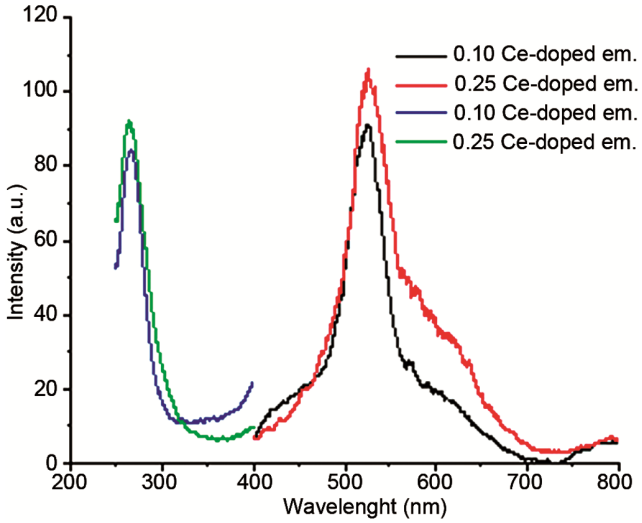

Fig. 7 — Photoluminescence spectra of 0.1% and 0.25 %, CeO_2-TiO_2 nanocomposite.

524 nm to 520 nm when the Ce^{3+} concentration increased from 0.1 mol% to 0.25 mol %. In other words, the blue shift of Ce^{3+} emission occurred when the concentration of Ce^{3+} ions was increased. According to this result, we can say that the 5d–4f transition Ce^{3+} is heavily dependent on the concentration of Ce^{3+} in the host crystal TiO_2.

4 Conclusions

We synthesized a novel spherical CeO_2 doped TiO_2 nanocomposites by a simple synthesis method.XRD data and crystallization parameters showed that crystallization powder samples took place. Surface and particle examinations showed that the particles had a regular distribution. According to PL studies, 0.1 mol% and 0.25 mol% CeO_2 doped TiO_2 phosphors have broad excitation band in the UV (200–300 nm) regions and a broad emission band located 400 nm to 700 nm. When factors affecting luminescence properties were investigated and discussed, the results showed that the blue shift of Ce^{3+} emission occurred when the concentration of Ce^{3+} ions was increased. The emission of Ce^{3+} is heavily dependent on the concentration of Ce^{3+} in the host crystal TiO_2. Furthermore, this study showed that 0.1 mol% and 0.25 mol% CeO_2 doped TiO_2 nanocomposite phosphors are economically good candidates for opto-electronic applications without rare earth element doping.

References

1 Shinar J, Organic Light-Emitting Devices, Springer, New York (2003).
2 Miller R D & Chandross E A, *Mater Electron Chem Rev*, 110 (2010) 1.
3 Koch N, *Chem Phys Chem*, 8 (2007) 1438.
4 Holm R H & O'Connor M J, *Prog Inorg Chem*, 14 (1971) 241.
5 Garnovskii A D, Nivorozhkin A L & Minkin V I, *Coord Chem Rev*, 126 (1993) 1.
6 Fujishima A, *Nature*, 238 (1972) 37.
7 Watanabe M, Hayashi T, Yagasaki H & Sasaki S, *Int J Mod Phys B*, 15 (2001) 3997.
8 Kaniyankandy S & Ghosh H N, *J Mat Chem*, 19 (2009) 3523.
9 Stevanovic A, Büttner M, Zhang Z & Yates J T, *J Am Chem Soc*, 134 (2012) 324.
10 Stepanov A L, *Rev Adv Mater Sci*, 30 (2012) 150.
11 Gomez P R, Palmero A, Ben T, Lozano J G, Molina S I & Gonzalez E A R, *Phys Rev B*, 82 (2010) 115420.
12 Dutta P K, Ginwalla A, Hogg B, Patton B R, Chwieroth B, Liang Z, *et al*., *J Phys Chem B*, 103 (1999) 4412.
13 Xu Y, Yao K, Zhou X & Cao Q, *Sens Actuators B*, 14 (1993) 492.
14 Phillips L G & Barbano D M, *J Dairy Sci*, 80 (1997) 2726.
15 Tryk D A, Fujishima A & Honda K, *Electrochim Acta*, 45 (2000) 2363.
16 Kuznetsov V N & Serpone N, *J Phys Chem C*, 113 (2009) 15110.
17 Naldoni A, Allieta M, Santangelo S, Marelli M, Fabbri F, Cappelli S, Bianchi C L, Psaro R & Santo V D, *J Am Chem Soc*, 134 (2012) 7600.
18 Liu X, Gao S, Xu H, Lou Z, Wang W, Huang B & Dai Y, *Nanoscale*, 5 (2013) 1870.
19 Chen X & Burda C, *J Am Chem Soc*, 130 (2008) 5018.
20 Yeh M S, Yang Y S, Lee Y P, Lee H F, Yeh Y H & Yeh C S, *J Phys Chem B*, 103 (1999) 6851.
21 Shahriari E, Yunus W M M & Saion E, *Braz J Phys*, 40 (2010) 256.
22 Ponce A A & Klabunde K J, *J Mol Catal A: Chem*, 225 (2005) 1.
23 Iranpoor N, Firouzabadi H, Safavi A, Motevalli S & Doroodmand M M, *Appl Organomet Chem*, 26 (2012) 417.
24 Kowlgi K, Lafont U, Rappolt M & Koper G, *J Colloid Interf Sci*, 372 (2012) 16.
25 Khan Z, Al-Thabaiti S A, Obaid A Y & Al-Youbi A O, *Colloids Surf B*, 82 (2011) 513.
26 Gomez P R, Palmero A, Ben T, Lozano J G, Molina S I & Gonzalez E A R, *Phys Rev B*, 82 (2010) 115420.
27 Bavykin D V, Friedrich J M & Walsh F C, *Adv Mater*, 18 (2006) 2807.
28 Chetibi L, Hamana D & Achour S, *Mater Chem Phys*, 144 (2014) 301.
29 Chunyan J, Liu B, Zhongxiang L & Jiaming S, *Nanoscale Res Lett*, 10 (2015) 1.
30 Chen J, Herricks T & Xia Y, *Chem Int Ed*, 44 (2005) 2589.
31 Uzun E, Öztürk E, Ozpozan K N & Karacaoglu E, *J Lumin*, 173 (2016) 73.
32 Öztürk E & Ozpozan K N, *J Therm Anal Calorim*, 117 (2014) 573.
33 Crossland E J W, Noel N, Sivaram V, Leijtens T, Alexander-Webber J A & Snaith H J, *Nature*, 495 (2013) 215.
34 Luo W Q, Li R F & Chen X Y, *J Phys Chem C*, 113 (2009) 8772.
35 Chang M Q, Song Y H, Zhang H G, Sheng Y, Zheng K Y, Zhou X Q & Zou H F, *RSC Adv*, 5 (2015) 59314.
36 Yoo J B, Yoo H J, Lim B W, Lee K H, Kim M H, Kang D & Hur N H, *ChemSusChem*, 5 (2012) 2334.
37 Stojadinovic S, Radic N, Grbic B, Maletic S, Stefanov P, Pacevski A & Rastko V R, *Appl Surf Sci*,70 (2016) 218.
38 Komaraiah D, Radha E, James J, Kalarikkal N, Sivakumar, J Ramana https://www.sciencedirect.com/science/article/pii/S0022231318315503 - !R M V & Sayanna R,https://www.sciencedirect.com/science/article/pii/S0022231318315503 - ! *J Lumin*, 211 (2019) 320.
39 Dokan F K & Kuru M, *Mater Sci: Mater Electron*, 32 (2021) 640.
40 Bokuniaeva A O & Vorokh A S, *J Phys Conf Ser*, 1410 (2019) 012057.
41 Muñoz-Batista M J, Gomez-Cerezo M N, Kubacka A, Tudela D & Fernandez-García M, *ACS Catal*, 4 (2014) 63.
42 Rožića L, Petrovića S, Lončarević D, Grbić B, Radić N, Stojadinović S, Jović V & Lamovec J, *Ceram Int*, 45 (2019) 2361.
43 Cano-Franco J C & lvarez-La´inez M A, *Mater Sci Semicond Process*, 90 (2019) 190.
44 Zhang F, Chan S W, Spanier J E, Apak E, Jin Q, Robinson R D & Herman I P, *Appl Phys Lett*, 80 (2002) 127.
45 Bersani D, Antonioli G, Lottici P P & Lopez T, *J Non Cryst Solids*, 175 (1998) 232.
46 Balachandran U & Eror N G, *J Solid State Chem*, 42 (1982) 276.
47 Lukačević I , Gupta S K , Jha P K & Kirin D , *Mater Chem Phys*, 137 (2012) 282.
48 Pallotti D K, Passoni L, Maddalena P, Fonzo F D & Lettieri S, *J Phys Chem C*, 121 (2017) 9011.
49 Stevanovic A & Yates J T, *J Phys Chem C*, 117 (2013) 24189.

50 Ma S, Reish M E, Zhang Z, Harrison I & Yates J T, *J Phys Chem C*, 121 (2017) 1263.
51 Oket A N & Yilmaz O, *Appl Catal A*, 354 (2009) 132.
52 Pavitra E, Raju G S R, Park W & Yu J S, *New J Chem*, 38 (2014) 163.
53 Bosze E J, McKittrick J & Hirata G A, *Mater Sci Eng B*, 97 (2003) 265.
54 Öztürk E & Sarılmaz E, *Mater Res Exp*, 6 (2019) 105710.
55 Uzun E, Öztürk E & Ozpozan K N, *Luminescence*, 33 (2018) 1346.
56 Öztürk E & Sarılmaz E, *Mater Chem Phys*, 239 (2020) 122085.
57 Öztürk E, Ozpozan K N & Uzun E, *J Chin Chem Soc*, 62 (2015) 47.
58 Fa-Chun Lu, Shu-Qing G, Zhi-Ping Y, Yan-Min Y, Pan-Lai L, Xu L & Quan-Lin L, *J Alloys Compd*, 521 (2012) 77.